

Surface Structure and Lattice Vibrations of MnO(001) Analyzed by High-resolution Medium Energy Ion Scattering Spectroscopy

Tetsuaki Okazawa and Yoshiaki Kido

Abstract

Clean MnO(001)-1×1 surfaces were successfully prepared by cleavage in N₂-ambience followed by annealing at 400°C for 20 min in O₂-pressure of 1×10⁻⁶ Torr. The rumpled relaxation and lattice dynamics of the MnO(001) surface was analyzed *in situ* by high-resolution medium energy ion scattering (MEIS) using 120 keV He⁺ ions. We determine the vertical displacements from the bulk lattice sites for the top- and 2nd-layer Mn and O atoms on the basis of the 3rd-layer Mn. It is found that the top-layer Mn atoms with a smaller polarizability are displaced toward the vacuum side relative to the top-layer O. This is consistent with the recent *ab initio* calculation but in conflict with the prediction based on the Coulombic interactions combined with a pair potential. Correlated thermal vibrations are also analyzed quantitatively by MEIS and the result obtained deviates largely from molecular dynamics simulations using the pair potential. The present result shows that the semi-classical treatment using pair potentials is no longer applicable to transition metal oxides with covalent bond and a fully quantum mechanical approach is required to calculate exact electron charge density distributions, which contribute to the force constant (corresponding to spring constant).

1. Introduction

Manganese monoxide (MnO) is a typical 3d antiferromagnetic insulator with the Néel temperature of 120 K. The electronic structure has been extensively investigated and revealed to be at a boundary between the Mott-Hubbard and charge-transfer regimes[1-3]. However, little is known about the surface structure. MnO takes a rock-salt structure with a lattice constant of 4.448 Å and the surface is very active for chemisorption. Only diffused LEED (low energy electron diffraction) patterns are observed for the MnO(001) cleaved in an ultrahigh vacuum (UHV). According to a literature[4], clear (1×1) spots are obtained by polishing followed by annealing at 480 K and the (1×1) patterns are transformed into (2×2) and (6×6) at temperatures between 800 and 1000 K but with no detectable change in surface stoichiometry. Recently, Langell et al.[5] reported that the MnO(001) surface annealed at 625 K in O₂-pressure of 5×10⁻⁷ Torr for 30 min showed the (1×1) LEED pattern and the extended annealing oxidized the surface gradually. Further annealing for 150 min led to formation of Mn₂O₃ surface. Namely, too high annealing temperature, too long annealing time and excess O₂-pressure promote oxidation. On the other hand, annealing in too low O₂-pressure would generate O-vacancies at the surface. So, it is difficult to prepare the clean MnO(001)-1×1 surface compared with the cases of NiO(001) and CoO(001)[4].

In this study, we clarify quantitatively the rumpled relaxation of the MnO(001)-1×1 surface and the thermal vibrations of the O and Mn atoms in the near surface region by high resolution medium energy ion scattering (MEIS). The ion shadowing and blocking effects[6] make it possible to determine directly in a real space the displaced lattice positions of the top- and 2nd-layer O and Mn atoms on the basis of the 3rd-layer Mn atoms. The ions incident along a major crystal axis hit the atoms even behind the top-layer atom in the crystal string due to thermal vibrations, which diminish the shadowing effect. Thus the hitting probability gives the information on the correlated thermal vibration amplitudes (TVA).

The aim of the present study is to test the validity of a recently reported *ab initio* calculations[7] of the rumpled relaxation of the transition metal oxides surfaces, which are in conflict with those predicted by semi-classical models using pair potentials[8]. Our previous work showed that Coulombic interactions combined with pair potentials reproduce well the rumpled surface structure as well as correlated thermal vibrations for alkali halide crystals such as RbI(001) and KI(001)[9,10]. For NiO(001), however, our MEIS analysis revealed that the top-layer Ni atoms were displaced toward the vacuum side relative to the top-layer O atoms[11]. It supports the above *ab initio* calculations. If one considers Coulombic interactions coupled with a pair potential, the top-layer atoms with a larger polarizability take an upper position relative to those with a smaller polarizability. Here, we must note that almost all alkali halide crystals have purely ionic nature and in contrast transition metal oxides have both ionic and covalent properties. It is interesting to see whether other transition metal oxide takes the surface structure predicted by the *ab initio* calculations or by

the semi-classical model using a pair potential. In order to clarify lattice dynamics quantitatively, we performed molecular dynamics (MD) simulations using pair potentials[9,12], which always predict strong and positive correlations between the nearest neighbor atoms in the [001]- and [101]-string. It was proved true for alkali halide crystals but not for NiO. So, it is also important to see whether pronounced correlations exist or not for MnO.

2. Experiment

A MnO(001) crystal rod with a purity better than 99.9 % was purchased from Earth Chemical Corporation.

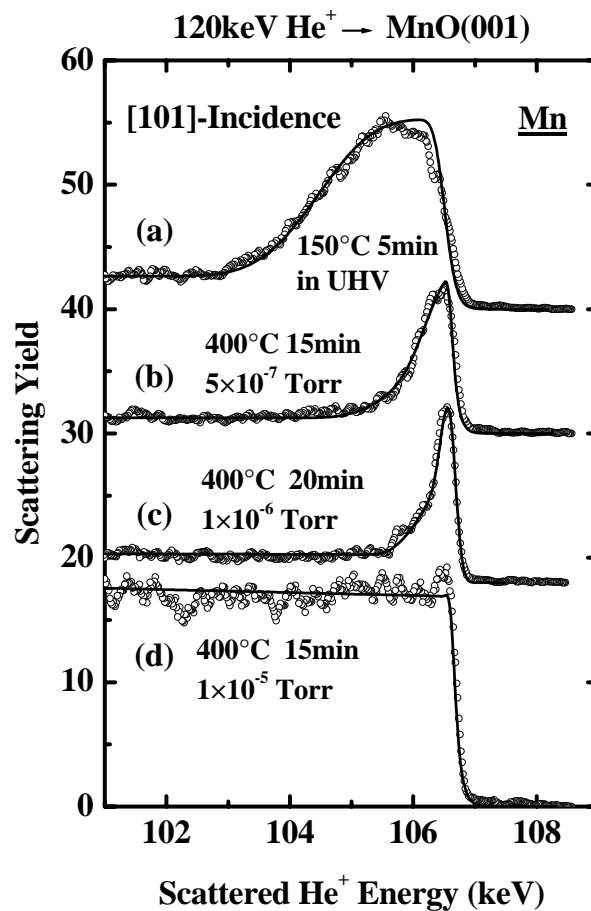


FIG. 1. MEIS spectra observed for 120 keV He⁺ incident along the [101]-axis and backscattered to 80° from Mn atoms. The samples were prepared by annealing at 150°C for 5 min in UHV (a), annealing at 400°C for 15 min in O₂-pressure of 5×10⁻⁷ Torr (b), annealing at 400°C for 20 min in O₂-pressure of 1×10⁻⁶ Torr (c) and annealing at 400°C for 15 min in O₂-pressure of 1×10⁻⁵ Torr (d). The solid curves are the best-fitted spectra assuming (a) damaged surface layers of 5-6 monolayers, (b) a surface with one damaged-layer, (c) a surface with no damaged layer and (d) a surface amorphized deeply.

A small piece with thickness of about 1 mm was cut from the above crystal rod with a razor blade in N₂-ambience and immediately introduced into a UHV chamber. In order to eliminate surface contaminations without generating O-vacancies at the surface, we annealed the samples in O₂-pressure of 1×10^{-7} to 1×10^{-4} Torr under a UHV condition. The clean (1×1) surface was confirmed by reflection high energy electron diffraction (RHEED) and Auger electron spectroscopy using 3 keV electron beams. MEIS experiment was performed *in situ* using 120 keV He⁺ ions. The scattered He⁺ ions were analyzed by a toroidal electrostatic spectrometer with an excellent energy resolution ($\Delta E / E$) of 9×10^{-4} , which gives a layer-by-layer depth resolution[13]. In order to avoid radiation damage, the irradiation area was slightly shifted after a He⁺ dose of 1 μ C.

Figure 1 shows the MEIS spectra observed for 120 keV He⁺ ions incident along the [101]-axis and backscattered to 80.0° (random direction) from MnO annealed at 150°C and 400°C in UHV and in different O₂-pressures. Annealing at 150°C for 5 min in UHV is insufficient to eliminate surface contaminations and to recover the surface layers damaged by cleavage. In fact, the RHEED observation shows a transmission pattern indicating a roughened surface. The surface crystallinity is considerably recovered but not completely by annealing at 400°C for 15 min in O₂-pressure of 5×10^{-7} Torr. The clean MnO(001)-1×1 surface was obtained by annealing at 400°C for 20 min in O₂-pressure of 1×10^{-6} Torr. The surface peak consists of primary two scattering components from the top- and 2nd-layer Mn atoms and the latter is significantly shadowed by the top-layer Mn atoms. In this case, RHEED observation showed a sharp (1×1) pattern and no carbon contamination was observed by AES and MEIS. Excess oxygen supply (1×10^{-5} Torr) led to amorphization, as indicated in Fig. 1 (d). We tested various conditions of annealing temperature, O₂-pressure and annealing time. As a result, the above condition (c) gives the best one to prepare a clean MnO(001)- 1×1 surface.

3. Results and Discussion

A. Surface Structure

Vertical displacements of the lattice site atoms from the ideal positions (bulk) are determined using the ion shadowing effect, if there is no surface reconstruction, namely no displacements in the lateral plane. Figure 2 shows the MEIS spectra observed for He⁺ ions incident along the [211]-axis and backscattered to 59° from Mn atoms. The [211]-string consists of only either Mn or O atoms. The shoulder part seen in the lower energy side consists of the scattering components mainly from the 2nd- and 3rd-layer of Mn atoms, as indicated by thin solid curves in Fig. 2. How to deconvolute a surface peak is referred to a literature[9,10].

Figure 3(a) shows angular scan spectra around the [211]-axis in the (1 $\bar{2}$ 0) plane for the scattering components mainly from the 2nd-layer of Mn atoms and from deeper layers of Mn. The angle (65.9°) giving a scattering yield minimum for the scattering component from deeper layers Mn

corresponds to the incidence along the [211]-axis of the bulk MnO crystal. The angular shift of -0.20° for the angles minimizing the above two scattering components determines the relative vertical distance between the top- and 2nd-layer of Mn atoms by a simple triangular method (see Fig. 4)[9].

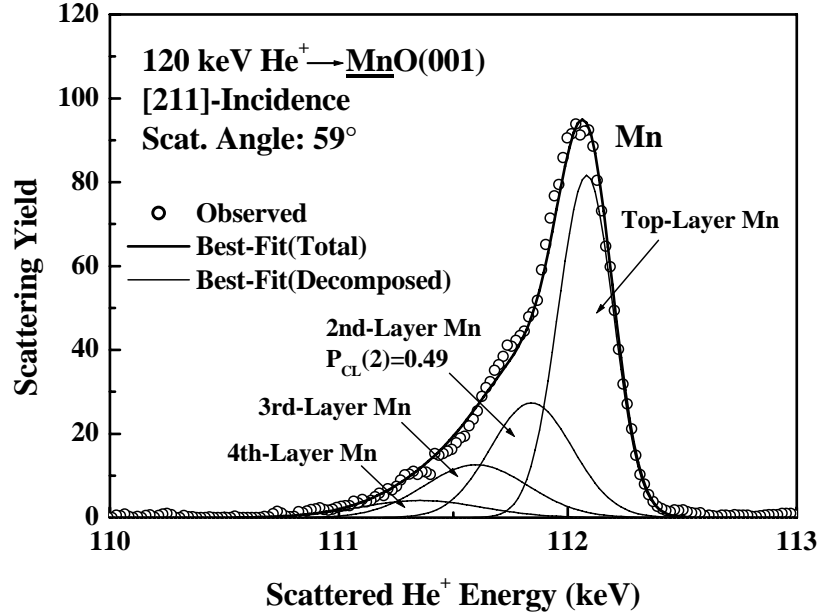


FIG. 2. MEIS spectrum (open circles) observed under the condition of [211] incidence and backscattering to 59° from Mn (random direction). The thick and thin solid curves are the best-fitted total and deconvoluted spectra from the top- down to the 4th-layer of Mn.

Similar polar scans were also performed around the $[111]$ -axis in the $(1\bar{1}0)$ plane for the scattering components mainly from the 2nd-, 3rd- and deeper layers of Mn atoms and from the 2nd- and deeper layers of O atoms, respectively, as shown in Figs. 3(b) and (c). In the $[111]$ -string, Mn and O atoms line up alternately. From the angular shifts, we obtain the vertical distances of the top- and 2nd-layer Mn and O atoms scaled from the 3rd-layer Mn atoms. The displacements of the top- and 2nd-layer lattice site positions, respectively on the basis of the 3rd-layer Mn are deduced to be $+0.02$ and 0.0 \AA for Mn and -0.06 and -0.045 \AA for O. Here, the plus sign means a displacement toward the vacuum side from the ideal lattice position (bulk). The present result shows that there is no significant relaxation in the first interlayer distance but the 2nd-interlayer distance is contracted by $1.0 \pm 0.7 \%$. Concerning the rumpling, the top- and 2nd-layer Mn atoms are significantly displaced toward the vacuum side relative to the respective O atoms. We performed the MD simulations using the pair potential proposed by Lewis and Catlow[8]. In the MD simulation, we used the dipole moments of the top- and 2nd-layer O atoms, which were estimated self-consistently only

employing the polarizability[14] to give the rumpled surface structure determined by MEIS[9,10]. The dipole moments of the Mn atoms are neglected, because the polarizability of Mn is much smaller than that of O[15]. In Table 1, the surface relaxation and rumpling determined here are compared with those predicted by the *ab initio* calculations[7] and MD simulation.

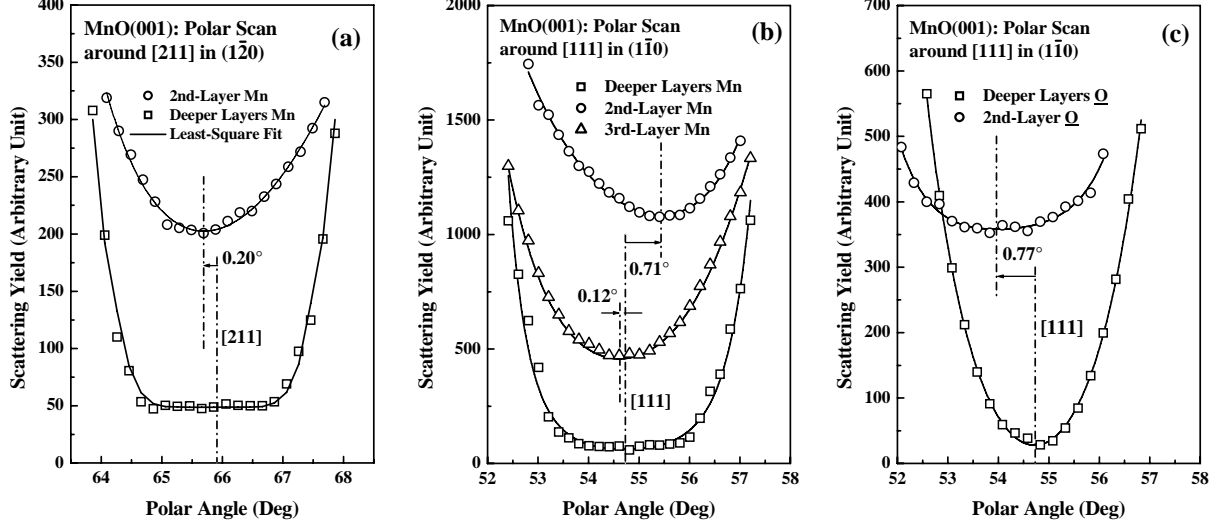


FIG. 3. (a) Polar scan spectra around the [211] axis in the $(\bar{1}\bar{2}0)$ plane for the scattering components mainly from the 2nd-layer Mn(circles) and from deeper layers Mn(squares). Solid curves denote least square polynomial fitting. (b) Polar scan spectra around the [111] axis in the $(\bar{1}\bar{1}0)$ plane for the scattering components mainly from the 2nd-layer Mn (circles), the 3rd-layer Mn (triangles) and deeper layers Mn (squares). (c) Polar scan around the [111] axis in the $(\bar{1}\bar{1}0)$ plane for the scattering components mainly from the 2nd-layer O (circles) and deeper layers O (squares).

The relaxation ($\varepsilon_{i,i+1}$) of the interlayer distance between the i th- and $(i+1)$ th-layer and the rumpling ($\Delta\varepsilon_i$) of the i th-layer are defined by

$$\begin{aligned}\varepsilon_{i,i+1} &= \{(d_{i,i+1} - d_{bulk}) / d_{bulk}\} \times 100 \quad (\%) \\ \Delta\varepsilon_i &= \{\Delta z(i) / d_{bulk}\} \times 100 \quad (\%) \end{aligned} \quad (1)$$

Here, $d_{i,i+1}$, d_{bulk} and $\Delta z(i)$, respectively are the interlayer distance between the i th- and $(i+1)$ th-layer, the bulk interlayer distance and the relative vertical-displacement of the anion (O^-) to cation (Mn^+) in the i th-layer. If one adopts Coulombic interactions coupled with pair potentials, the top-layer atoms with a larger polarizability take an upper position rather than those with a smaller polarizability. Polarizability can be extracted from optical refraction data. Actually, the present MEIS result supports the *ab initio* calculations rather than the semi-classical treatment. This situation is quite similar to that for NiO(001)[11]. It must be noted that pair potentials have basically an isotropic nature and reflect almost isotropic electron charge density, which holds for

ionic crystals.

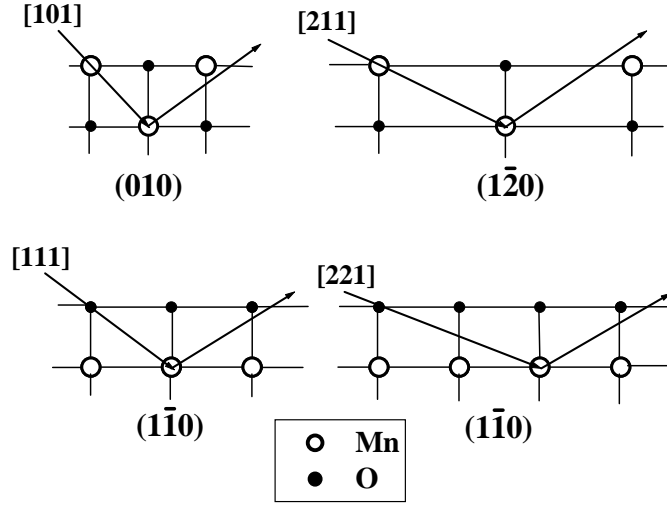


FIG. 4. Side views of various kinds of scattering geometries.

For covalent crystals, however, there is an accumulation of electrons between the bonding atoms. In such a case, a fully quantum mechanical treatment is required to calculate exact electron charge density distributions, which contribute to a force constant (corresponding to a spring constant). Transition metal oxides such as NiO and MnO have both ionic and covalent bonding. This is the reason why the relaxation and rumpling for NiO(001) and MnO(001) can be predicted by the first principle calculations not by the semi-classical theory using pair potentials.

Table 1. Surface relaxation ($\varepsilon_{i,i+1}$) and rumpling ($\Delta\varepsilon(i)$) determined by MEIS are compared with those predicted by the *ab initio* calculations[7] and semi-classical MD simulation.

| | $\varepsilon_{1,2}(\%)$ | $\varepsilon_{2,3}(\%)$ | $\Delta\varepsilon(1)(\%)$ | $\Delta\varepsilon(2)(\%)$ |
|------------------|-------------------------|-------------------------|----------------------------|----------------------------|
| MEIS | $+0.1 \pm 0.7$ | -1.0 ± 0.7 | -3.6 ± 0.7 | $+2.0 \pm 0.7$ |
| <i>Ab initio</i> | -1.4 | -0.3 | -0.5 | -1.4 |
| MD | -2.9 | +1.6 | +1.7 | -1.6 |

B. Lattice Dynamics

The ion shadowing effect also provides the information about correlated thermal vibrations. For example, the probability to hit a 2nd-layer atom for ions incident along a major crystal axis is estimated from the root mean square (rms) TVAs of the top and 2nd-layer atoms along with the correlation between them in the direction perpendicular to the incident beam axis[6]. Here, we

must note that the TVAs of near surface atoms are significantly enhanced in particular in surface normal direction. Of course, the TVA of the top-layer atoms in surface normal direction is most strongly enhanced. Concerning the correlations, the larger the atomic spacing, the smaller the correlation. In the present analysis, as a first approximation, we consider only the enhancement of the TVAs of the top-layer atoms in surface normal direction and the correlations between the nearest neighbor atoms in the direction perpendicular to the [001]- and [101]-axis.

It is known from Monte Carlo simulations of ion trajectories that the polar scan profile around a major crystal axis for the scattering components from enough deep layers atoms is dependent primarily on the bulk thermal TVAs and not sensitive to the enhancements and correlations. Figure 5 shows the polar scan profile around the [211] axis in the $(1\bar{2}0)$ plane for the scattering components mainly from the 5th- down to 8th-layer Mn atoms. The corresponding energy window was set to the region from 110.1 to 111.1 keV (see Fig. 2). Apparently, assumption of the bulk TVA of 0.09 \AA gives the best-fit to the observed polar scan spectrum with uncertainty of 0.005 \AA .

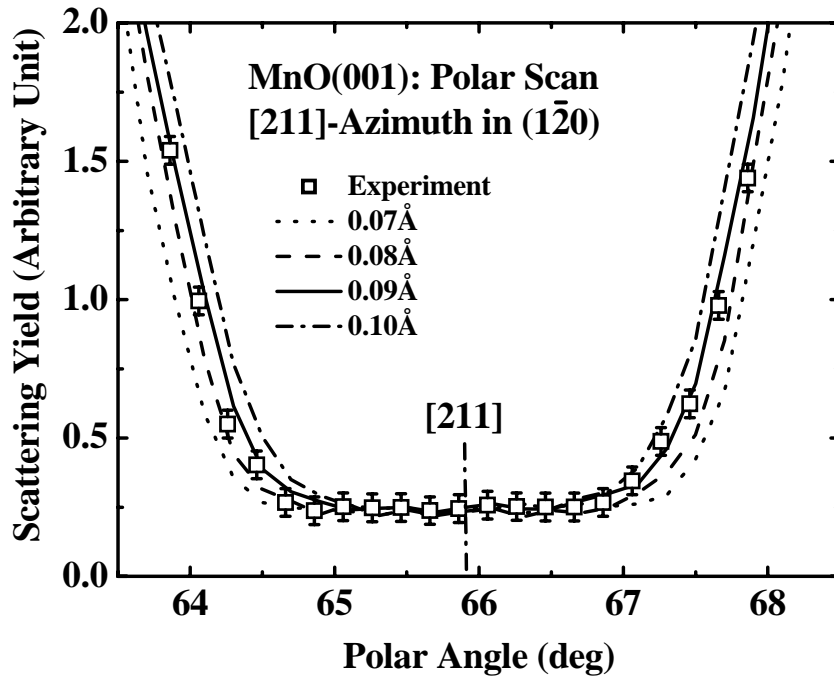


FIG. 5. Observed (squares) and simulated (curves) polar scan spectra around the [211]-axis in the $(1\bar{2}0)$ plane for scattering components mainly from the fifth- to eighth-layer Mn atoms. The corresponding energy window was put between 110.1 and 111.1 keV. The detection direction was fixed to 55° from the surface normal. Vertical scale denotes the total scattering yield from the above energy range divided by the scattering yield from the top-layer Mn atoms (see Fig. 2). Correction is made considering the scattering cross section dependent on scattering angle.

The enhancement of the TVA of the top-layer Mn is derived from the hitting probability of the 2nd-layer of Mn for the [211]-incidence. Now, we introduce the concept of close encounter probability $P_{CL}(n)$ for a n th-layer atoms, which is obtained experimentally by normalizing the scattering yield from the n th-layer atoms by that from the top-layer atoms. It is equivalent to the hitting probability of the n th-layer atoms divided by that of the top-layer atoms, which is calculated from the Monte Carlo simulation of ion trajectories[6,9]. The close encounter probability for the 2nd-layer Mn in the [211]-string is derived to be 0.49 by deconvoluting the surface peak, as indicated in Fig. 2. If one assumes no correlations between the Mn atoms in the [211]-string and an enhancement (β_{Mn}) of the top-layer Mn in surface normal direction, one can calculate the normalized hitting probability, namely close encounter probability $P_{CL}^{Mn}(n)$ for the n th-layer Mn atoms. Here, enhancement coefficient β is defined by $\langle u_{\perp} \rangle = \beta \langle u_{bulk} \rangle$, where $\langle u_{\perp} \rangle$ and $\langle u_{bulk} \rangle$ are an enhanced TVA in surface normal direction and the TVA of the bulk, respectively. The β_{Mn} value is derived to be 2.4 ± 0.1 to give the above $P_{CL}^{Mn}(2)$ value of 0.49.

In order to obtain the TVAs of the bulk and the top-layer O atoms, we measured MEIS spectra under the following two scattering geometries, (i) [111]-incidence and backscattering to 64° (random direction) and (ii) [221]-incidence and backscattering to 48.5° (random direction).

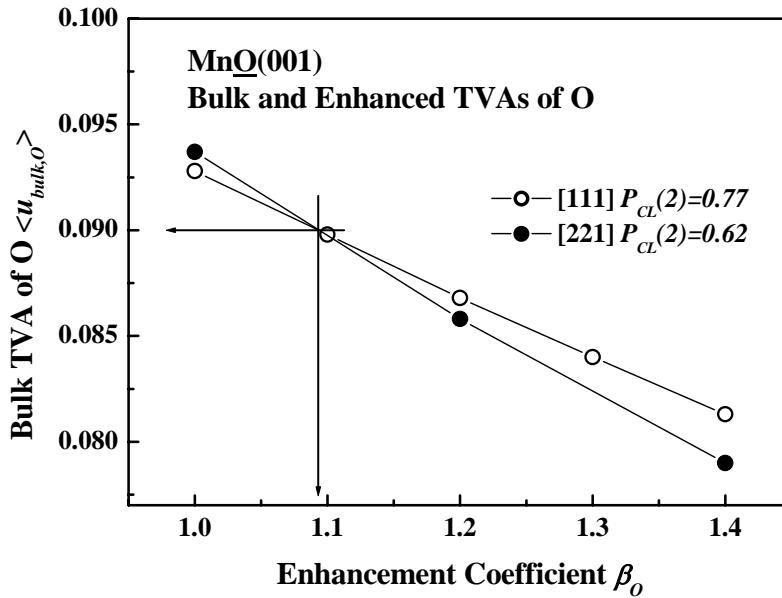


FIG. 6. Points satisfying the close encounter probabilities ($P_{CL}^{Mn}(2)=0.77$ for [111]-incidence and $P_{CL}^{Mn}(2)=0.62$ for [221]-incidence) for the 2nd-layer Mn atoms. The crossing point gives the $\langle u_{bulk,O} \rangle$ and β_o values.

The $P_{CL}^{Mn}(2)$ values for the above two scattering geometries are 0.77 and 0.62, respectively. In this case, there are two unknown factors (fitting parameters), the bulk and enhanced TVAs of O atoms

(see Fig. 4). Figure 6 indicates the combination of ($\beta_O, \langle u_{bulk,O} \rangle$) to give the above two $P_{CL}^{Mn}(2)$ values. The crossing point in Fig. 6 corresponds to just the values to be determined. Thus we obtain the β_O value of $1.1_{+0.3}^{-0.1}$ and $\langle u_{bulk,O} \rangle$ value of $0.090 \pm 0.01 \text{ \AA}$. It is interesting that β_O is much smaller than β_{Mn} . This suggests that the TVA of the top-layer Mn atoms taking an upper position relative to the top-layer O is much more enhanced. Such a situation is also seen for NiO(001)[11]. The bulk TVAs give the individual Debye temperature(Θ), if one simply employs the Debye model, although it can be applied only to monatomic solids. The deduced Debye temperatures for Mn and O are 340 ± 30 K and 620 ± 50 K, respectively. Hofmann et al.[16] measured the temperature-dependent heat capacity of MnO and derived the individual Debye temperatures of 350 K for Mn and 700 K for O, which were conveniently introduced for thermodynamic analysis. The individual Debye temperatures deduced from MEIS analysis are compatible with those derived from the above heat capacity measurement. The present MD simulation gives the TVAs of 0.059 and 0.060 \AA for bulk Mn and O, respectively and the enhancement coefficients of 1.23 and 1.24 for the top-layer Mn and O, respectively. Large deviations of the MD simulations from the MEIS result indicates inapplicability of the semi-classical MD simulation to MnO, as quite similar to NiO[11].

Finally, we determine the correlation coefficient between the nearest neighbor atoms in the [001]- and [101]-string. The correlation coefficient C_{ij} is defined by

$$C_{ij} = \frac{\langle u_i \cdot u_j \rangle}{\sqrt{\langle u_i \cdot u_i \rangle \langle u_j \cdot u_j \rangle}}, \quad (2)$$

where u_i is the displacement of an atom i from its equilibrium position and the bracket means a time average. In the MEIS analysis, the direction of the correlated motion is taken to be perpendicular to the incident beam axis. Figure 7 shows the MEIS spectra observed under the condition of the [001]-incidence and backscattered to the [601]-direction in the (010) plane. The $P_{CL}^{Mn}(2)$ value is derived to be 0.53 by the spectrum deconvolution, which is given assuming the correlation coefficient (C_{O-Mn}^{001}) of $+0.08 \pm 0.1$ between the top-layer O and the 2nd-layer Mn in the direction perpendicular to the [001]-axis. We also measured the MEIS spectrum for the [101]-incidence and backscattered to 80.0° . From the $P_{CL}^{Mn}(2)$ value of 0.60, the correlation coefficient C_{Mn-Mn}^{101} in the direction perpendicular to the [101]-axis is deduced to be 0.0 ± 0.1 . Thus we find no correlations within systematic errors for MnO, as quite similar to NiO. In contrast, the present MD simulation gives large correlations of $+0.31$ and $+0.22$ as C_{O-Mn}^{001} and C_{Mn-Mn}^{101} , respectively. In the previous MEIS analysis for RbI(001) and KI(001), we found strong positive correlations between neighboring atoms in the [001]- and [101]-string, which were consistent with those calculated from the MD simulations using pair potentials[9,10]. The large discrepancies

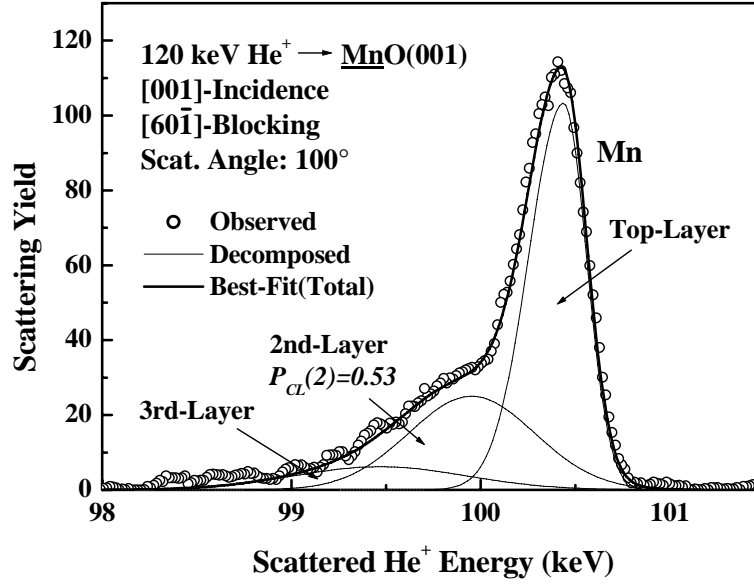


FIG. 7. MEIS spectrum observed for [001]-incidence and emergence along the $[60\bar{1}]$ -axis. Thick and thin solid curves, respectively are the best-fitted total and decomposed spectra to the observed one.

between the MEIS analysis and the MD simulations for MnO and NiO show that the semi-classical treatments using pair potentials are no longer applicable to transition metal oxides which have both ionic and covalent bonds. The reason why pair potentials is inapplicable to materials with covalent bonds is ascribed to their pronounced anisotropic charge distributions of valence electrons in contrast to purely ionic materials.

Table 2. Correlated TVAs of Mn and O determined by MEIS and calculated from MD.

| | $\langle u_{bulk,Mn} \rangle$ | $\langle u_{bulk,O} \rangle$ | β_{Mn} | β_O | C_{O-Mn}^{001} | C_{Mn-Mn}^{101} |
|------|-------------------------------|------------------------------|---------------|---------------------|------------------|-------------------|
| MEIS | $0.088 \pm 0.005 \text{ \AA}$ | $0.090 \pm 0.01 \text{ \AA}$ | 2.4 ± 0.1 | $1.1_{+0.3}^{-0.1}$ | 0.08 ± 0.1 | 0.0 ± 0.1 |
| MD | 0.059 \AA | 0.060 \AA | 1.23 | 1.24 | +0.31 | +0.22 |

4. Summary

The clean MnO(001)- 1×1 surface was successfully prepared by cleavage in N_2 ambience followed by annealing at 400°C for 20 min in O_2 -pressure of 1×10^{-6} Torr. Too high annealing temperature, too long annealing time and excess O_2 -pressure promote oxidation and finally lead to amorphization. On the other hand, annealing in too low O_2 -pressure generates O-vacancies at the surface. The rumpled relaxation and the correlated thermal vibrations were analyzed *in situ* by

high-resolution MEIS. We first determined the vertical displacements from the bulk lattice sites for the top- and 2nd-layer Mn and O atoms on the basis of the 3rd-layer Mn. Outward displacement of the top-layer Mn atoms with a smaller polarizability compared with the O atoms is consistent with the *ab initio* calculations but in conflict with the prediction by the semi-classical treatment using the pair potential.

The ion shadowing effect makes it also possible to determine the correlated thermal vibrations. The bulk TVAs of Mn and O are derived to be 0.088 ± 0.005 and 0.090 ± 0.01 Å and the enhancements in surface normal direction of the top-layer Mn and O are 2.4 ± 0.1 and $1.1^{+0.1}_{-0.3}$, respectively. The above MEIS result largely deviates from the MD calculations using the pair potential. As quite similar to NiO and alkali halide crystals, the semi-classical MD simulations predict large and positive correlations between the nearest neighbor atoms in the [001]- and [101]-string. However, the present MEIS analysis shows no significant correlations for MnO(001), as quite similar to NiO(001).

We must note that pair potentials have basically an isotropic nature and reflect almost isotropic electron charge density, which is valid for ionic crystals. For covalent crystals, however, there is an accumulation of electrons between the bonding atoms. Thus, in particular, for covalent crystals a fully quantum mechanical treatment is required to calculate exact electron charge density distributions, which contribute to the force constant (corresponding to spring constant). Transition metal oxides such as NiO and MnO have both ionic and covalent bonding. This is the reason why the rumpled surface structure and correlated thermal vibrations for NiO(001) and MnO(001) cannot be predicted by the semi-classical theory using pair potentials.

Acknowledgments

The authors would like to thank Dr. Y. Hoshino for assistance in carrying out the MEIS experiment. Thanks are also due to Y. Nakagawa and I. Kato for their help in analysis of the MEIS data.

References

- [1] J.M. McKay, M.H. Mohamed and V. E. Henrich, Phys. Rev. **B 35** (1987) 4304.
- [2] R.J. Lad and V.E. Henrich, Phys. Rev. **B 38** (1988) 10860.
- [3] A. Fujimori, N. Limizuka, T. Akahane, T. Chiba, S. Kimura, F. Minami, K. Siratori, M. Taniguchi, S. Ogawa and S. Suga, Phys. Rev. **B 42** (1990) 7580.
- [4] V.E. Henrich and P.A. Cox, 'The surface science of metal oxides' (Cambridge Univ. Press, 1994, Cambridge).
- [5] M.A. Langell, C.W. Hutchings, G.A. Carson and M.H. Nassir, J. Vac. Sci. Technol. **A 14**

- (1996) 1656.
- [6] J.F. van der Veen, *Surf. Sci. Rep.* **5** (1985) 199.
- [7] H. Momida and T. Oguchi, *J. Phys. Soc. Jpn.* **72** (2003) 588.
- [8] G.V. Lewis and C.R.A. Catlow, *J. Phys.* **C 18** (1985) 1149.
- [9] T. Okazawa, T. Nishimura and Y. Kido, *Phys. Rev.* **B 66** (2002) 125402.
- [10] Y. Kido and T. Okazawa, *Surf. Rev. Lett.* **10** (2003) 389.
- [11] T. Okazawa, Y. Yagi and Y. Kido, *Phys. Rev.* **B 67** (2003) 195406.
- [12] T. Okazawa, S. Ohno, Y. Hoshino, T. Nishimura and Y. Kido, *Nucl. Instrum. Methods* **B 183** (2001) 108.
- [13] Y. Kido, T. Nishimura, Y. Hoshino and H. Namba, *Nucl. Instrum. Methods* **B 161-163** (2000) 371.
- [14] R.R. Peddy, Y.N. Ahammed, P.A. Azeem and K.R. Gopal, *J. Non-Cryst. Solids* **286** (2001) 169.
- [15] K.S. Upadhyaya, G.K. Upadhyaya and A.N. Pandey, *J. Phys. Chem. Solids* **63** (2002) 127.
- [16] J.A. Hofmann, A. Paskin, K.J. Tauer and R.J. Weiss, *J. Phys. Chem. Solids* **1** (1956) 45.